J. Fluid Mech. (1988), *vol.* 195, *pp.* 201–221
Printed in Great Britain

Trapping and resonance of long shelf waves due to groups of short waves

By YEHUDA AGNON† AND CHIANG C. MEI‡

† Department of Mathematics, Massachusetts Institute of Technology, Cambridge, MA 02139, USA

‡ Department of Civil Engineering, Massachusetts Institute of Technology, Cambridge, MA 02139, USA

(Received 25 March 1987 and in revised form 4 January 1988)

Groups of short waves within a narrow frequency band are known to be accompanied by second-order long waves travelling at the group velocity of the predominant short waves. When the short waves are refracted by bottom topography, new long waves can be further radiated and propagated away from the topography at the shallow-water speed. Since over a long submarine ridge there can be trapped modes of long-period waves, incident groups of short waves can excite the trapped waves through a second-order mechanism. In this paper we study such excitations over a rectangular shelf which scatters the first-order short waves. By employing asymptotic methods we examine the transient excitation of the trapped long wave by both sinusoidal wave groups and wave packets. The effects of a small angular spread of the incident waves are also included.

1. Introduction and formulation

It is well known in the linearized theory of long water waves in shallow water that simple harmonic waves of certain frequencies can be trapped on a long shelf or on a ridge (Longuet-Higgins 1967). In the idealized case of an infinitely long ridge such waves cannot be excited linearly by simple harmonic waves approaching the ridge from outside; they can only be generated by local forcing such as overhead wind.

For ridges of oceanographic interest, the trapped wavelength can be comparable with the width of the ridge. The corresponding periods are typically a few minutes, which are much longer than the typical wind-wave periods of $O(10$–20 s), but close to the modulational periods of swell groups. The goal of this paper is to show that narrow-banded wind waves incident from the sea can excite trapped long waves on a shelf through a nonlinear mechanism. Both steady and transient wave groups will be considered.

Nonlinear interaction of waves with topography, with particular emphasis on wave trapping, has been studied by Foda & Mei (1981) and by Mei & Benmoussa (1984) for cases where the water depth changes slowly in space so that reflection of the short waves is negligible. In the present work we shall consider the case where reflection of the short waves is significant. Particular attention will be paid to transient resonance. For demonstration of the physics, we choose a relatively simple bathymetry of a rectangular shelf as shown in figure 1. Cartesian coordinates

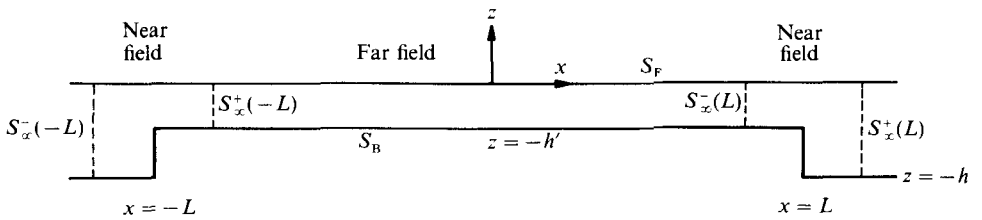

FIGURE 1. The ridge geometry.

(x, y, z) are chosen so that the rest position of the free surface is the (x, y) plane with z positive upwards. The bathymetry is given by

$$\left.\begin{aligned} &\text{depth} = h \quad (|x| > L, \quad -\infty < y < \infty),\\ &\text{depth} = h' \quad (|x| < L, \quad -\infty < y < \infty),\end{aligned}\right\} \tag{1.1}$$

where

$$h > h'. \tag{1.2}$$

Thus the ridge runs parallel to the y-axis. We assume that the water is of intermediate depth: $\sigma h = O(1)$; $\sigma h' = O(1)$ where

$$\sigma \equiv \omega^2/g = k \tanh kh. \tag{1.3}$$

k is the central wavenumber and ω is the central frequency of the short waves. The half-width of the ridge, L, is assumed to be comparable with the length of the wave groups; and very long compared with the short-wave length, i.e.

$$kL = O(\epsilon^{-1}) \gg 1, \quad \Delta k/k = O(\epsilon) \ll 1. \tag{1.4}$$

Only waves of small slope will be considered. To study the most interesting cases where nonlinearity and dispersion are comparable, we take the characteristic slope of the short waves ka to be $O(\epsilon)$ also.

The governing equations for the velocity potential are

$$\nabla^2 \Phi = \Phi_{xx} + \Phi_{yy} + \Phi_{zz} = 0 \quad \text{in the fluid,} \tag{1.5}$$

$$\Phi_{tt} + g\Phi_z = \left[-\tfrac{1}{2}(\nabla\Phi)^2 + \frac{1}{g}\Phi_t \Phi_{zt} \right]_t - \nabla_h \cdot (\nabla_h \Phi \Phi_t) + O(\nabla_h \Phi^3, (\Phi^3)_t), \quad z = 0, \tag{1.6}$$

where $\nabla_h \equiv (\partial_x, \partial_y)$, and,

$$\left.\begin{aligned} \Phi_z = 0, \quad z = -h' \quad (|x| < L),\\ = -h \quad (|x| > L),\end{aligned}\right\} \tag{1.7}$$

$$\Phi_x = 0 \quad (x = \pm L, \quad -h < z < -h'). \tag{1.8}$$

As in Agnon & Mei (1985) we introduce the slow coordinates

$$(x_1, y_1, t_1) = \epsilon(x, y, t) \tag{1.9}$$

and the following expansion:

$$\Phi = \sum_{n=1}^{\infty} \epsilon^n \sum_{m=-n}^{n} \Phi_{nm} \, \mathrm{e}^{-\mathrm{i}m\omega t}, \tag{1.10}$$

where

$$\Phi_{nm} = \Phi_{nm}(x, y, z, x_1, y_1, t_1), \quad \Phi_{nm} = \Phi^*_{n,-m}. \tag{1.11}$$

In this expansion Φ_{11} represents the short-period waves at the leading order, and Φ_{10} is the long-period wave potential. The perturbation equations governing Φ_{nm} can be straightforwardly deduced (Agnon & Mei 1985), and will be cited when needed.

Our approach may be outlined as follows. At the leading order, the short waves are found by the solutions of a linear diffraction problem, which has been studied by Newman (1965), Miles (1967) and Mei & Black (1969). At the next order we examine separately the near field within a few swell lengths of the shelf edge, and the far field a few group lengths away from the edge. After first finding the forms of the potentials for the long waves in each field, we match their asymptotic values with the near fields to get the final result. As in Mei & Benmoussa (1984) who studied only a slowly varying topography, two types of long waves are shown to exist. The first one is locked to the short-wave groups and propagates at the group velocity. The other is a shallow-water wave generated at the shelf edges. For nearly normal incidence it propagates both on the shelf and outwards in directions different from those of the short waves and of the locked long waves; the speed of propagation is the local velocity of long waves. Under certain conditions of oblique incidence, long waves of the second type can be trapped and resonated on the shelf. Responses to sinusoidally modulated and transient wave groups are analysed. The effects of a small directional spread are also included for generality. As a matter of notation, we denote the potential in the near field by ψ, i.e.

$$\Phi \equiv \psi, \quad k(x \pm L) \leqslant O(1), \tag{1.12}$$

and the potential in the far field by ϕ:

$$\Phi \equiv \phi, \quad k(x_1 - L_1) = O(1); \quad k(x_1 + L_1) = O(1). \tag{1.13}$$

For convenience we shall use $L_1 \equiv \epsilon L$ to denote the scaled half-width of the shelf when we refer to the x_1 coordinate. First, let us examine the first-order short-wave potentials in the near and far fields, ψ_{11} and, ϕ_{11}.

2. The potential for sinusoidally modulated short waves

In the near field of each shelf edge, the equations for ψ_{11} are formally the same as the equations for the diffraction of regular waves by a rectangular step (Miles 1967). To account for diffraction by the whole shelf one must combine ψ_{11} with the far field ϕ_{11} over the shelf. Two alternative approaches can be taken. On the one hand we may spectrally decompose the narrow-banded incident wave into a discrete set of sinusoidal components and superpose the respective solutions for the total diffraction field. Alternatively, short waves may be regarded as being sinusoidal with slowly varying envelopes. For sinusoidal modulation where the spectrum is composed of two frequencies, the first approach is simpler.

Consider now a strictly sinusoidal wavetrain. In view of the wide-shelf assumption (1.4) it is most convenient to employ an approximation due to Newman (1965), by taking into account only the propagating modes for the interaction between the two edges, and ignoring the evanescent modes. Since the results are crucial to our later analysis, we sketch Newman's reasoning below. Consider first the left edge $x = -L$ of a step of infinite width. Let the potential of a wave incident from $x \sim -\infty$ (from deep to shallow water) have the amplitude A, i.e.

$$\psi_{11}^{\mathrm{I}} = A f_0 \exp(\mathrm{i}\alpha x + \mathrm{i}\gamma y) \quad (x < -L), \tag{2.1a}$$

with

$$\alpha = k\cos\theta; \quad \gamma = k\sin\theta; \tag{2.1b}$$

where θ is the angle of incidence, and

$$f_0(z) = \frac{\sqrt{2}\cosh k(z+h)}{(h+\sigma^{-1}\sinh^2 kh)^{\frac{1}{2}}}. \tag{2.1c}$$

the free-surface amplitude a of the incident wave is related to the potential amplitude A by

$$a = \frac{2i\omega}{g} f_0(0)\, A. \tag{2.2}$$

Then the propagating modes of the reflected and transmitted waves are given by

$$\psi_{11}^{\mathrm{R}} = ARf_0 \exp(-i\alpha x + i\gamma y) \quad (x < -L), \tag{2.3a}$$

$$\psi_{11}^{\mathrm{T}} = ATf_0' \exp(i\alpha' x + i\gamma y) \quad (x > -L), \tag{2.3b}$$

respectively, with $k'^2 = \alpha'^2 + \gamma^2$; k' and f_0' are related to h' in the same way as k and f_0 to h. The total propagating-wave potential is

$$\left.\begin{aligned} \psi_{11} &= \psi_{11}^{\mathrm{I}} + \psi_{11}^{\mathrm{R}} \quad \text{for } x < -L, \\ \psi_{11} &= \psi_{11}^{\mathrm{T}} \quad \text{for } x > L. \end{aligned}\right\} \tag{2.4}$$

R and T denote the reflection and transmission coefficients for a wave incident from the deep side $x+L \sim -\infty$ toward the step. The values of R and T can be determined numerically by the Galerkin method (Garrett 1971) or the closely related variational method (Miles 1967 or Mei & Black 1969). We then consider the right edge of the shelf and calculate the scattered wave due to an incident wave from the right (shallow side) toward a step of infinite width. The corresponding coefficients of reflection (to the right) and transmission (to the left) are denoted by R' and T' respectively. The numerical results have been checked against published theories as well as the exact law of energy conservation:

$$(1-|R|^2) C_{\mathrm{g}} \cos\theta = |T|^2 C_{\mathrm{g}}' \cos\theta', \tag{2.5}$$

where $\tan\theta' = \gamma/\alpha'$.

Now we make use of these coefficients R, T, R' and T' for a step to a shelf of large but finite width. The short-wave potential in the far fields outside the shelf can be expressed as

$$\phi_{11} = (A\, e^{i\alpha x + i\gamma y} + B\, e^{-i\alpha x + i\gamma y}) f_0 \qquad (x < -L), \tag{2.6a}$$

$$\phi_{11} = (C\, e^{i\alpha x + i\gamma y}) f_0 \qquad (x > L); \tag{2.6b}$$

and on the shelf as

$$\phi_{11} = (D\, e^{i\alpha' x + i\gamma y} + E\, e^{-i\alpha' x + i\gamma y}) f_0' \qquad (|x| < L). \tag{2.6c}$$

Matching the propagating modes in (2.3) and (2.4) and making use of the reflection and transmission coefficients for each step, we immediately get

$$\left.\begin{aligned} RA\, e^{i\alpha(-L)} + T'E\, e^{-i\alpha'(-L)} &= B\, e^{-i\alpha(-L)}, \\ TA\, e^{i\alpha(-L)} + R'E\, e^{-i\alpha'(-L)} &= D\, e^{i\alpha'(-L)} \end{aligned}\right\} \quad \text{at } x = -L, \tag{2.7a, b}$$

and

$$\left.\begin{aligned} T'D\, e^{i\alpha' L} &= C\, e^{i\alpha L}, \\ R'D\, e^{i\alpha' L} &= E\, e^{-i\alpha' L} \end{aligned}\right\} \quad \text{at } x = L. \tag{2.7c, d}$$

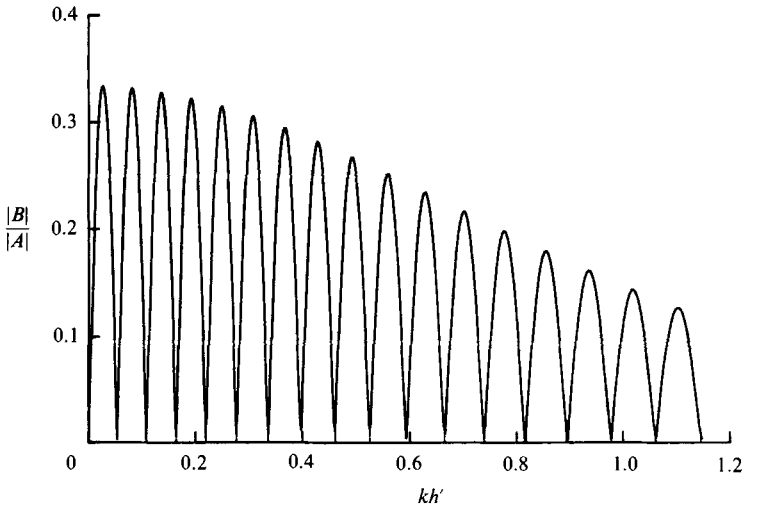

FIGURE 2. The reflection coefficient $|B/A|$ for a ridge versus kh'; $h'/h = 0.5$; $L/h = 10$; normal incidence ($\theta = 0$).

Solution of these simultaneous equations yields B, C, D, and E:

$$\begin{Bmatrix} B \\ C \\ D \\ E \end{Bmatrix} = \frac{A}{1-R'^2\,\mathrm{e}^{4\mathrm{i}\alpha' L}} \begin{Bmatrix} R'\,\mathrm{e}^{-\mathrm{i}\alpha L} + R'TT'\,\mathrm{e}^{\mathrm{i}(4\alpha'-\alpha)L} \\ T'T\,\mathrm{e}^{2\mathrm{i}(\alpha'-\alpha)L} \\ T\,\mathrm{e}^{\mathrm{i}(\alpha'-\alpha)L} \\ R'T\,\mathrm{e}^{\mathrm{i}(3\alpha'-\alpha)L}. \end{Bmatrix} \tag{2.8}$$

This result is due to Newman (1965).

Numerical values of $|B/A|$, are plotted *vs.* kh' in figure 2. The variations of $|C/A|$, $|D/A|$ and $|E/A|$ are similar and are omitted. By considering all evanescent modes, accurate solutions for B–E can also be calculated by using a variational method (Mei & Black 1969). Numerical agreement with Newman's wide-shelf approximation has been found to be excellent for the parameters considered. Note that since kL is large, interference is strong and a small change in k results in a large change in B, C, D and E.

Consider now an incident wave which is the sum of two monochromatic waves slightly detuned from the central frequency, α and γ, i.e.

$$\phi_{11}^{\mathrm{I}}\,\mathrm{e}^{-\mathrm{i}\omega t} = f_0(z)\,[A^+\,\mathrm{e}^{\mathrm{i}(\alpha^+ x+\gamma^+ y-\omega^+ t)} + A^-\,\mathrm{e}^{\mathrm{i}(\alpha^- x+\gamma^- y-\omega^- t)}]\,\mathrm{e}^{-\mathrm{i}\omega t}, \tag{2.9a}$$

where

$$\alpha^\pm = \alpha \pm \epsilon\mu\Omega, \quad \gamma^\pm = \gamma \pm \epsilon\nu\Omega, \quad \omega^\pm = \omega \pm \epsilon\Omega. \tag{2.9b}$$

A^+ and A^- may be different in general. Equation (2.9a) can be alternatively written as

$$\phi_{11}^{\mathrm{I}}\,\mathrm{e}^{-\mathrm{i}\omega t} = \{A\,\mathrm{e}^{\mathrm{i}(\alpha x+\gamma y-\omega t)}\} f_0(z), \tag{2.10a}$$

with

$$A = A^+\,\mathrm{e}^{-\mathrm{i}\Omega(t_1-\mu x_1-\nu y_1)} + A^-\,\mathrm{e}^{\mathrm{i}\Omega(t_1-\mu x_1-\nu y_1)}. \tag{2.10b}$$

For strictly sinusoidal modulation A^+ and A^- are equal constants, in which case they will be taken to be related to the maximum free-surface amplitude a by (2.2).

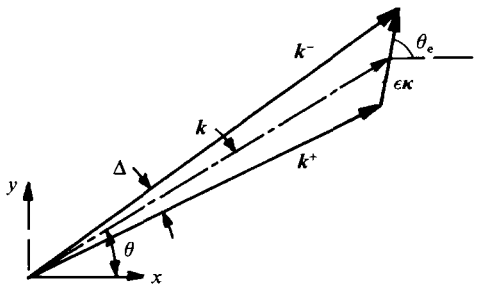

FIGURE 3. The wavenumber vectors $\boldsymbol{k}$, $\boldsymbol{k}^+$ and $\boldsymbol{k}^-$ where $\boldsymbol{k}^+ = (\alpha^+, \gamma^+)$ and $\boldsymbol{k}^- = (\alpha^-, \gamma^-)$.

For the incident envelope we shall define $\epsilon\boldsymbol{\kappa}$ as its wavenumber vector and θ_e its direction, with

$$\boldsymbol{\kappa} = \Omega(\mu, \nu)/C_g, \quad \theta_e = \tan^{-1}\frac{\nu}{\mu}. \tag{2.11}$$

These are depicted in figure 3. From the dispersion relation (1.3) one can show that

$$1 = C_g(\alpha\mu + \gamma\nu)/k \quad \text{or} \, \Omega = C_g\kappa\cos(\theta - \theta_e). \tag{2.12}$$

The difference in angles of the two trains

$$\begin{aligned} \Delta &= \tan^{-1}\frac{\gamma + \epsilon\Omega\nu}{\alpha + \epsilon\Omega\mu} - \tan^{-1}\frac{\gamma - \epsilon\Omega\nu}{\alpha - \epsilon\Omega\mu} \\ &\approx \frac{2\epsilon\Omega}{k^2}(\alpha\nu - \gamma\mu) = \frac{2\epsilon\Omega}{kC_g}\tan(\theta_e - \theta) \end{aligned} \tag{2.13}$$

is the directional spread of the total incident wave. The range of $\theta_e - \theta$ is $(-\frac{1}{2}\pi, \frac{1}{2}\pi)$. For $\theta_e - \theta = \pm\frac{1}{2}\pi$, there is no modulation in time. If the two uniform wavetrains in (2.9*a*) are collinear, $\theta_e = \theta$ and

$$\frac{\nu}{\mu} = \frac{\gamma}{\alpha}, \tag{2.14}$$

and μ and ν are further related by

$$1 = C_g(\mu^2 + \nu^2)^{\frac{1}{2}}, \text{ i.e. } \Omega = C_g\kappa. \tag{2.15}$$

the propagation speed of the incident envelope is in general

$$C_e = \frac{\Omega}{\kappa} = C_g\cos(\theta - \theta_e) = \frac{1}{(\mu^2 + \nu^2)^{\frac{1}{2}}}. \tag{2.16}$$

When two uniform wavetrains are collinear, $C_e = C_g$.

Now each wavetrain in (2.6*a*, *b*) can be represented in the form of (2.10). By superposition we have the envelopes of the scattered waves:

$$\begin{Bmatrix} B \\ C \end{Bmatrix} = \begin{Bmatrix} B^+ \\ C^+ \end{Bmatrix}\exp[-i\Omega(t_1 \pm \mu x_1 - \nu y_1)] + \begin{Bmatrix} B^- \\ C^- \end{Bmatrix}\exp[i\Omega(t_1 \pm \mu x_1 - \nu y_1)]. \tag{2.17}$$

On the shelf, the two refracted wavetrains must have the same γ and ν. The x-component is now $\pm\alpha'$ for the wave and $\pm\mu$ for the envelope. The component μ' can be found from (2.12):

$$\mu' = \frac{\alpha}{\alpha'}\mu + \frac{1}{\alpha'}\left(\frac{k'}{C_g'} - \frac{k}{C_g}\right). \tag{2.18}$$

In the limit of collinear waves (2.14) holds; (2.18) reduces to

$$\Omega\mu' = \frac{\kappa}{k}\left[\alpha' + \frac{k'^2}{\alpha'}\left(\frac{k}{k'}\frac{C_g}{C_g'} - 1\right)\right]. \tag{2.19}$$

This formula applies also to a slowly varying bottom (Mei & Benmoussa 1984, equation (3.9) where C_0/C_{g_0} should be corrected as C_{g_0}/C_0). Now the envelopes of the combined waves on the shelf are

$$\begin{Bmatrix} E \\ D \end{Bmatrix} = \begin{Bmatrix} E^+ \\ D^+ \end{Bmatrix} \exp\left[-i\Omega(t_1 \pm \mu' x_1 - \nu y_1)\right] + \begin{Bmatrix} E^- \\ D^- \end{Bmatrix} \exp\left[i\Omega(t_1 \pm \mu' x_1 - \nu y_1)\right]. \tag{2.20}$$

The coefficients $B^\pm$, $C^\pm$, $D^\pm$, and $E^\pm$ are related to $A^\pm$, $R^\pm$, $T^\pm$, $R'^\pm$, $T'^\pm$, $\alpha^\pm$, and $\alpha'^\pm$ just as B, C, D, and E are to A, R, T, R', T', α and α' in (2.8). Because $(\alpha^+ - \alpha^-)L$ is of order unity, the rapid oscillations in figure 3 imply that B^+ and B^-, etc. can differ significantly.

We now turn to the long-wave potential. Unless otherwise stated the component wavetrains of the incident waves are not assumed to be collinear.

3. Long-wave potential for incident short waves with a sinusoidal envelope

3.1. *The far fields*

Accounting for oblique incidence in accordance with (2.2), we can easily modify (4.7) in Agnon & Mei (1985) to get the governing equation for the long waves in water of depth h:

$$\phi_{10_{t_1t_1}} - gh\nabla_1^2\phi_{10} = -f_0^2(0)\left(k^2 - \sigma^2 + \frac{2\omega k}{C_g}\right)(|P|^2 + |Q|^2)_{t_1}, \quad |x_1| > L_1, \tag{3.1a}$$

where $\nabla_1 = (\partial/\partial x_1, \partial/\partial y_1)$. Over the shelf, $|x_1| < L_1$, a similar equation holds with h, k, C_g and f_0 replaced by h', k', C_g' and f_0, respectively. P and Q are the potential amplitudes of waves propagating to the right and to the left respectively.

Specifically

$$P = \begin{cases} A, \\ D, \\ C, \end{cases} \quad Q = \begin{cases} B & (x_1 < -L), \\ E & (|x_1| < L_1), \\ 0 & (x_1 > L_1). \end{cases} \tag{3.1b}$$

Note that only the self-interaction of each propagating wavetrain contributes to the long-wave potential ϕ_{10}. Short waves propagating in opposite x-directions contribute only to short-scale oscillations and have zero mean. In view of (2.10) and (2.12), $|P|^2$ and $|Q|^2$ in (3.1) consist of zeroth and second harmonics in slow timescales. Specifically, corresponding to a typical right-going short wave in the deeper water we have

$$|A|^2 = |A^+|^2 + |A^-|^2 + 2\,\mathrm{Re}\left[A^+A^{-*}\,\mathrm{e}^{-2i\Omega(t_1 - \mu x_1 - \nu y_1)}\right] \equiv |A^+|^2 + |A^-|^2 + \widetilde{|A|^2}. \tag{3.2a}$$

The expression for C is similar. For the left-going short wave B, we have instead

$$|B|^2 = |B^+|^2 + |B^-|^2 + 2\,\mathrm{Re}\left[B^+B^{-*}\,\mathrm{e}^{-2i\Omega(t_1 + \mu x_1 - \nu y_1)}\right] \equiv |B^+| + |B^-|^2 + \widetilde{|B|^2}. \tag{3.2b}$$

For later convenience, we denote by $\widetilde{|A|^2}$ the oscillatory part of $|A|^2$. By changing μ to μ', the corresponding relations for D and E can be written. Forced by these harmonics as in (3.1), ϕ_{10} must contain the same harmonics. Physically, the zeroth-harmonic part of ϕ_{10} corresponds to steady set-up or set-down, while the second-

harmonic part is oscillatory. We shall only consider the more interesting second harmonic. The corresponding solution to (3.1) is further split into two parts. One part is the inhomogeneous solution which is not required to satisfy any boundary conditions. It is easy to see that the inhomogeneous solution in two depths can be separated according to the wave-trains and propagate at the respective group velocities. For any envelope Z in deep water, the *locked* long wave is given by

$$\phi_{10}^{(Z)} = \mathrm{Re}\,\mathscr{Z}\,\mathrm{e}^{-2\mathrm{i}\Omega(t_1 \mp \mu x_1 - \nu y_1)}, \tag{3.3}$$

$$\{\mathscr{Z}\} = \begin{Bmatrix} \mathscr{A} \\ \mathscr{B} \\ \mathscr{C} \end{Bmatrix} = \begin{Bmatrix} A^+ A^{-*} \\ B^+ B^{-*} \\ C^+ C^{-*} \end{Bmatrix} \frac{m}{-2\mathrm{i}\Omega}, \tag{3.4a}$$

where

$$m = 2\frac{f_0(0)\,C_\mathrm{e}^2}{gh - C_\mathrm{e}^2}\left(k^2 - \sigma^2 + \frac{2\omega k}{C_\mathrm{g}}\right) \tag{3.4b}$$

is independent of Ω. In (3.3), the minus sign in the exponent is associated with the right-going envelopes $Z = (A, C)$, and the plus sign with the left-going group $Z = B$. The long waves locked to the wave envelopes on the shelf, $Z = (D, E)$, have expressions similar to (3.3) and (3.4), where h, k, C_e and μ must be replaced by h', k', C_e' and μ' respectively.

The remaining oscillatory part of ϕ_{10} corresponds to solutions to the homogeneous equation:

$$\left.\begin{aligned} \phi^\mathrm{F}_{10t_1t_1} - gh\,\nabla_1^2\phi^\mathrm{F}_{10} = 0 \quad (|x_1| > L_1), \\ \phi^\mathrm{F}_{10t_1t_1} - gh'\,\nabla_1^2\phi^\mathrm{F}_{10} = 0 \quad (|x_1| < L_1); \end{aligned}\right\} \tag{3.5}$$

hence they will be called the *free* long waves, denoted by the superscript F. The sum of the inhomogeneous and homogeneous solutions must satisfy certain boundary conditions. In particular ϕ^F_{10} must be either outgoing or vanishing at $|x_1| \to \infty$. The latter corresponds to long waves trapped on the shelf.

Because the potentials for the locked long waves are periodic in y_1, the free waves must be likewise. We shall be mostly interested in trapped free waves and hence will denote the x_1 (cross-shelf) wavenumbers of the free waves by $2\mathrm{i}\Omega\beta$ for $|x_1| > L_1$ and $2\Omega\beta'$ for $|x_1| < L_1$ where β and β' are different from μ and μ' and must satisfy

$$-\beta^2 + \nu^2 = (gh)^{-1}, \quad \beta'^2 + \nu^2 = (gh')^{-1}. \tag{3.6}$$

For trapping it is necessary that β and β' be real so that

$$-\beta^2 = \frac{1}{gh} - \nu^2 < 0 < \beta'^2 = \frac{1}{gh'} - \nu^2: \tag{3.7}$$

Now the free wave ϕ^F_{10} must be of the form

$$\phi^\mathrm{F}_{10} \equiv \phi^G_{10} = \mathrm{Re}\,\mathscr{G}\,\mathrm{e}^{-2\mathrm{i}\Omega(t_1 - \nu y_1) + 2\Omega\beta x_1} \quad (x_1 < -L_1), \tag{3.8a}$$

$$\phi^\mathrm{F}_{10} \equiv \phi^H_{10} + \phi^K_{10} \quad (|x_1| < L_1), \tag{3.8b}$$

with

$$\phi^H_{10} = \mathrm{Re}\,\mathscr{H}\,\mathrm{e}^{-2\mathrm{i}\Omega(t_1 - \beta' x_1 - \nu y_1)}, \tag{3.8c}$$

$$\phi^K_{10} = \mathrm{Re}\,\mathscr{K}\,\mathrm{e}^{-2\mathrm{i}\Omega(t_1 + \beta' x_1 - \nu y_1)}, \tag{3.8d}$$

and

$$\phi^\mathrm{F}_{10} \equiv \phi^J_{10} = \mathrm{Re}\,\mathscr{J}\,\mathrm{e}^{-2\mathrm{i}\Omega(t_1 - \nu y_1) - 2\Omega\beta x_1} \quad (x_1 > L_1). \tag{3.8e}$$

The total long-wave potential is obtained by adding the locked and the free long waves

$$\left.\begin{aligned}\phi_{10} &= \phi_{10}^{A}+\phi_{10}^{B}+\phi_{10}^{G} && (x_1 < -L_1),\\ \phi_{10} &= \phi_{10}^{D}+\phi_{10}^{E}+\phi_{10}^{H}+\phi_{10}^{K} && (|x_1| < L_1),\\ \phi_{10} &= \phi_{10}^{C}+\phi_{10}^{J} && (x_1 > L_1).\end{aligned}\right\} \tag{3.9}$$

The rays of these long waves are sketched in figure 4. The coefficients $\mathscr{G}$, $\mathscr{H}$, $\mathscr{K}$, and $\mathscr{J}$ will be determined by matching the total slow-wave potential in the near fields of the edges, to which we must now turn.

3.2. *The near fields*

In the near field of an edge, the variation of ψ_{10} with respect to x, y and z is governed by the Laplace equation and zero normal-flux conditions on $z = 0$ and along the boundaries of the step. This has been shown formally by Agnon & Mei (1985, equations (4.1)) and is expected intuitively. Consequently, the slow potential ψ_{10} is independent of short scale (x, y, z). However, it must depend on y_1 owing to variations of the incident waves

$$\psi_{10} = \psi_{10}(y_1, t_1), \quad x_1 \sim -L_1 \quad \text{or} + L_1. \tag{3.10}$$

It should be stressed that while ψ_{10} does not depend on x_1, there is still a second-order slow drift velocity in the x-direction. As in Agnon & Mei (1985, equation (4.22)) ψ_{20} is governed by

$$\left(\frac{\partial^2}{\partial x^2}+\frac{\partial^2}{\partial z^2}\right)\psi_{20} = 0 \quad (-h < z < 0), \tag{3.11}$$

$$\frac{\partial \psi_{20}}{\partial z} = -\frac{1}{g}\left[\mathrm{i}\omega\psi_{11}^{*}\psi_{11x}+*\right]_x \equiv h\frac{\partial U}{\partial x} \quad (z = 0), \tag{3.12}$$

$$\left.\begin{aligned}\frac{\partial \psi_{20}}{\partial z} = 0 \quad & (z = -h, x < -L),\\ & (z = -h' x > -L),\end{aligned}\right\} \tag{3.13}$$

$$\frac{\partial \psi_{20}}{\partial x} = 0 \quad (-h < z < -h', \quad x = -L). \tag{3.14}$$

The velocity U defined in (3.12) is just Stokes' drift. Integrating the normal derivative of ψ_{20} around the boundaries of the near field of the left edge, i.e. $S_{\infty}^{+}, S_{\infty}^{-}$, S_{B} and S_{F} (see figure 1) we find

$$\int_{S_{\infty}^{+}(-L)} \psi_{20x}\,\mathrm{d}z - \int_{S_{\infty}^{-}(-L)} \mathrm{d}z = -[h'U(-L+\infty)-hU(-L-\infty)], \tag{3.15}$$

where $S_{\infty}^{\pm}$ stand for the outer limits to the right and to the left of the edge at $x = -L$.

Near the right edge, we have, similarly,

$$\int_{S_{\infty}^{+}(L)} \psi_{20x}\,\mathrm{d}z - \int_{S_{\infty}^{-}(L)} \psi_{20x}\,\mathrm{d}z = -[hU(L+\infty)-h'(U(L-\infty)]. \tag{3.16}$$

The derivation of (3.15) and (3.16) is very similar to the one encountered in our parallel analysis of a floating body in beam seas (Agnon & Mei 1985; see the first of

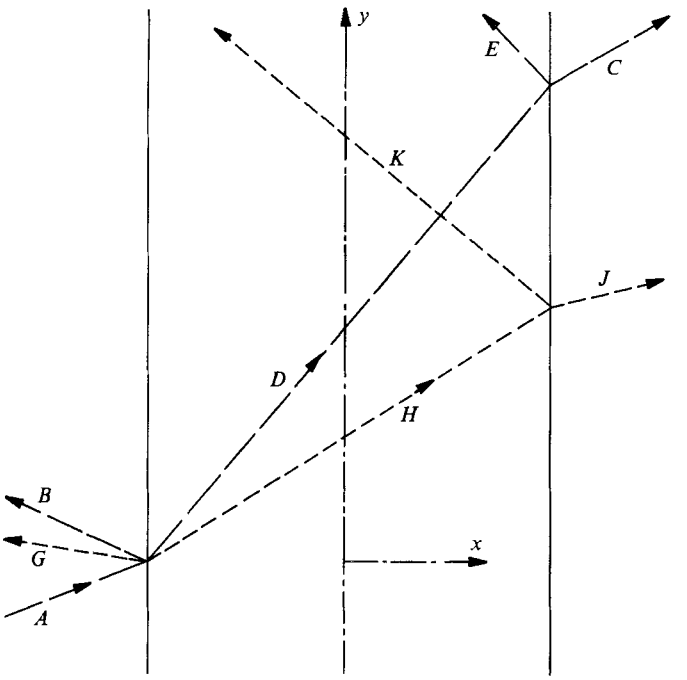

FIGURE 4. Rays of long waves over a ridge: ——, group-locked waves; - - - - -, free waves. The directions are $\mathrm{d}y/\mathrm{d}x = \pm 1/C_g$ off the ridge and $\pm 1/C'_g$ on the ridge for group-locked waves; $\pm 1/(gh)^{\frac{1}{2}}$ off the ridge and $\pm 1/(gh)^{\frac{1}{2}}$ on the ridge for free waves.

(4.24) where $f_0^2(0)$ should be multiplied). Explicit formulas for Stokes' drift can be worked out straightforwardly:

$$\left.\begin{aligned} hU(-L-\infty) &= h\,\mathrm{Re}\,\mathscr{U}^{(1)}\,\mathrm{e}^{-2\mathrm{i}\Omega t_1} \equiv \frac{2\omega\alpha}{g} f_0^2(0)\,(|A|^2-|B|^2) && (x_1 = -L_1-0),\\ h'U(-L+\infty) &= h'\,\mathrm{Re}\,\mathscr{U}^{(2)}\,\mathrm{e}^{-2\mathrm{i}\Omega t_1} \equiv \frac{2\omega\alpha'}{g} f_0'^2(0)\,(|D|^2-|E|^2) && (x_1 = -L_1+0),\\ h'U(L-\infty) &= h'\,\mathrm{Re}\,\mathscr{U}^{(3)}\,\mathrm{e}^{-2\mathrm{i}\Omega t_1} \equiv \frac{2\omega\alpha'}{g} f_0'^2(0)\,(|D|^2-|E|^2) && (x_1 = L_1-0),\\ hU(L+\infty) &= h\,\mathrm{Re}\,\mathscr{U}^{(4)}\,\mathrm{e}^{-2\mathrm{i}\Omega t_1} \equiv \frac{2\omega\alpha}{g} f_0^2(0)\,|C|^2 && (x_1 = L_1+0). \end{aligned}\right\} \quad (3.17)$$

3.3. *Matching of near and far fields and free long waves*

We now approximate ϕ_{10} to gets its inner expansion

Left edge:

$$\phi_{10} \sim \{\phi_{10}^A + \phi_{10}^B + \phi_{10}^G\} + (x_1+L_1)\{[-\mu\phi_{10}^A + \mu\phi_{10}^B]_{t_1} + \phi_{10x_1}^G\} \quad (x_1 \to -L_1-0); \quad (3.18a)$$

$$\phi_{10} \sim \{\phi_{10}^D + \phi_{10}^E + \phi_{10}^H + \phi_{10}^K\} + (x_1+L_1)\{-\mu'\phi_{10}^D + \mu'\phi_{10}^E - \beta'\phi_{10}^H + \beta'\phi_{10}^K\}_{t_1} \quad (x_1 \to -L_1+0); \quad (3.18b)$$

where all quantities in { } are evaluated at $x_1 = -L_1$.

Right edge:

$$\phi_{10} \sim \{\phi_{10}^D+\phi_{10}^E+\phi_{10}^H+\phi_{10}^K\} + (x_1-L_1)\{-\mu'\phi_{10}^D+\mu'\phi_{10}^E-\beta'\phi_{10}^H-\beta'\phi_{10}^K\}_{t_1} \quad (x_1\to L_1-0); \tag{3.18c}$$

$$\phi_{10} \sim \{\phi_{10}^C+\phi_{10}^J\}+(x_1-L_1)\{-\mu\phi_{10t_1}^C+\phi_{10x_1}^J\} \quad (x_1\to L_1+0); \tag{3.18d}$$

where all quantities in { } are evaluated at $x_1 = L_1$.

Use has been made of the simple relations between t_1 and x_1 derivatives of the propagating modes. For example, we have

$$\frac{\partial}{\partial x_1}=\mu\frac{\partial}{\partial t_1} \quad \text{for } \phi_{10}^A \quad \text{and } \phi_{10}^C, \quad \frac{\partial}{\partial x_1}=\beta'\frac{\partial}{\partial t_1} \quad \text{for } \phi^{\mathrm{K}} \text{ etc.},$$

and similar relations for left-going waves with a change of sign. Matching the long-wave potentials across an edge through ψ_{10} (cf. (3.10)) we get

$$\phi_{10}^A+\phi_{10}^B+\phi_{10}^G=\psi_{10}^-=\phi_{10}^D+\phi_{10}^E+\phi_{10}^H+\phi_{10}^K \quad (x_1=-L_1), \tag{3.19a}$$

$$\phi_{10}^D+\phi_{10}^E+\phi_{10}^H+\phi_{10}^K=\psi_{10}^+=\phi_{10}^C+\phi_{10}^J \quad (x_1=L_1). \tag{3.19b}$$

In (3.18), the coefficients of $(x_1 \pm L_1)$ correspond to mass fluxes associated with the long waves. Matching the fluxes terms in (3.18) with the near-field flux

$$\int_{S_\infty^\pm}\psi_{20_x}\,\mathrm{d}z$$

and making use of (3.15) we get

$$h[-\mu\phi_{10t_1}^A+\mu\phi_{10t_1}^B+\phi_{10x_1}^G]-h'[-\mu'\phi_{10}^D+\mu'\phi_{10}^E-\beta'\phi_{10}^H+\beta'\phi_{10}^K]_{t_1} = h'U(-L+\infty)-hU(-L-\infty) \quad (x_1=-L_1), \tag{3.19c}$$

$$h'[-\mu'\phi_{10}^D+\mu'\phi_{10}^E-\beta'\phi_{10}^H+\beta'\phi_{10}^K]_{t_1}-h[-\mu\phi_{10t_1}^C+\phi_{10x_1}^J] = hU(L+\infty)-h'U(L-\infty) \quad (x_1=L_1). \tag{3.19d}$$

When (3.2), (3.3) and (3.8) are substituted into (3.19) we obtain a linear matrix equations for $\mathscr{G}, \mathscr{H}, \mathscr{K}$, and $\mathscr{J}$.

$$\boldsymbol{N}\begin{Bmatrix}\mathscr{G}\\ \mathscr{H}\\ \mathscr{K}\\ \mathscr{J}\end{Bmatrix}=\begin{Bmatrix}a_1\\ a_2\\ a_3\\ a_4\end{Bmatrix}, \tag{3.20}$$

where the matrix $\boldsymbol{N}$ is given by

$$\boldsymbol{N}=\begin{bmatrix} \mathrm{e}^{-2\Omega\beta L_1} & -\mathrm{e}^{-2\mathrm{i}\Omega\beta' L_1} & -\mathrm{e}^{2\mathrm{i}\Omega\beta' L_1} & 0 \\ 0 & \mathrm{e}^{2\mathrm{i}\Omega\beta' L_1} & \mathrm{e}^{-2\mathrm{i}\Omega\beta' L_1} & -\mathrm{e}^{-2\Omega\beta L_1} \\ 2\Omega h\beta\,\mathrm{e}^{-2\Omega\beta L_1} & -2\mathrm{i}\Omega h'\beta'\,\mathrm{e}^{-2\mathrm{i}\Omega\beta' L_1} & 2\mathrm{i}\Omega h'b'\,\mathrm{e}^{2\mathrm{i}\Omega\beta' L_1} & 0 \\ 0 & 2\mathrm{i}\Omega h'\beta'\,\mathrm{e}^{2\mathrm{i}\Omega\beta' L_1} & -2\mathrm{i}\Omega h'\beta'\,\mathrm{e}^{-2\mathrm{i}\Omega\beta' L_1} & 2\Omega h\beta\,\mathrm{e}^{-2\Omega\beta L_1} \end{bmatrix}, \tag{3.21}$$

and a_1, a_2, a_3, and a_4 are related to the locked wave components in (3.18):

$$\left.\begin{aligned}
a_1 &= -\mathscr{A}\,\mathrm{e}^{-2\mathrm{i}\Omega\mu L_1} - \mathscr{B}\,\mathrm{e}^{2\mathrm{i}\Omega\mu L_1} + \mathscr{D}\,\mathrm{e}^{-2\mathrm{i}\Omega\mu' L_1} + \mathscr{E}\,\mathrm{e}^{2\mathrm{i}\Omega\mu' L_1},\\
a_2 &= \mathscr{C}\,\mathrm{e}^{2\mathrm{i}\Omega\mu L_1} - \mathscr{E}\,\mathrm{e}^{-2\mathrm{i}\Omega\mu' L_1} - \mathscr{D}\,\mathrm{e}^{2\mathrm{i}\Omega\mu' L_1},\\
a_3 &= -h[(-\mu\mathscr{A}\,\mathrm{e}^{-2\mathrm{i}\Omega\mu L_1} + \mu\mathscr{B}\,\mathrm{e}^{2\mathrm{i}\Omega\mu L_1})(-2\mathrm{i}\Omega) + \mathscr{U}^{(1)}]\\
&\quad + h'[(-\mu'\mathscr{D}\,\mathrm{e}^{-2\mathrm{i}\Omega\mu' L_1} + \mu'\mathscr{E}\,\mathrm{e}^{2\mathrm{i}\Omega\mu' L_1})(-2\mathrm{i}\Omega) + \mathscr{U}^{(2)}],\\
a_4 &= -h'[(\mu'\mathscr{E}\,\mathrm{e}^{-2\mathrm{i}\Omega\mu' L_1} - \mu'\mathscr{D}\,\mathrm{e}^{2\mathrm{i}\Omega\mu' L_1})(-2\mathrm{i}\Omega) + \mathscr{U}^{(3)}]\\
&\quad + h[-\mu\mathscr{C}\,\mathrm{e}^{2\mathrm{i}\Omega\mu L_1}(-2\mathrm{i}\Omega) + \mathscr{U}^{(4)}].
\end{aligned}\right\} \tag{3.22}$$

Equation (3.20) can be solved to yield a full solution for the long waves.

We now examine the physical implications of the solutions. The matrix $\boldsymbol{N}$ in (3.21) becomes singular when its determinant vanishes, i.e.

$$(\beta h + \mathrm{i}\beta' h')^2\,\mathrm{e}^{4\mathrm{i}\Omega\beta' L_1} - (\beta h - \mathrm{i}\beta' h')^2\,\mathrm{e}^{-4\mathrm{i}\Omega\beta' L_1} = \mathrm{Im}\,[(\beta h + \mathrm{i}\beta' h')^2\,\mathrm{e}^{4\mathrm{i}\Omega\beta' L_1}] = 0, \tag{3.23}$$

which is the known eigenvalue condition for trapped modes on a rectangular shelf according to the linearized shallow-water wave theory. In particular, (3.23) may be solved to give the nth eigenfrequency Ω_n:

$$2\Omega_n \beta' L_1 = \tan^{-1}\frac{\beta h}{\beta' h'} + \tfrac{1}{2}n\pi. \tag{3.24}$$

For collinear incident wavetrains, ν is determined from (2.14) and (2.15). For non-collinear trains one may prescribe the angular spread Δ; ν and μ are then determined from (2.12) and (2.13). In either case β and β' follow from (3.6) and the nth eigenfrequency Ω_n is then given by (3.24). For even (or odd) n, the free-surface profile associated with the trapped long wave Φ_{10} is symmetric (or antisymmetric) about the longitudinal axis ($x = 0$) of the shelf (see Mei 1983, p. 140).

We note that the second and third columns of (3.21) are complex conjugates of each other. This means that

$$\mathscr{H}(2\Omega) = -\mathscr{H}^*(2\Omega). \tag{3.25}$$

Hence the free wave on the shelf is of the form

$$\begin{aligned}
&\mathrm{Re}[\mathscr{H}\,\mathrm{e}^{-2\mathrm{i}\Omega(t_1 - \beta' x_1 - \nu y_1)} - \mathscr{H}^*\,\mathrm{e}^{-2\mathrm{i}\Omega(t_1 + \beta' x_1 - \nu y_1)}]\\
&\qquad = |\mathscr{H}|\sin(2\Omega\beta' x_1 - \arg\mathscr{H})\cos 2\Omega(t_1 - \nu y_1),
\end{aligned} \tag{3.26}$$

which is a wave standing in the x_1 direction, and propagating in the y_1 direction.

The standing-wave amplitude $\mathscr{H}$ is found from (3.20) by matrix inversion

$$\mathscr{H} = \frac{\mathbf{M}_{\mathscr{A}}}{\mathrm{Im}\,[(\beta h + \mathrm{i}\beta' h')^2\,\mathrm{e}^{4\mathrm{i}\Omega\beta' L_1})]\,4\Omega^2} = \frac{\mathbf{M}_{\mathscr{A}}}{[(\beta h)^2 + (\beta' h')^2]\,4\Omega^2 \sin 4\beta' L_1(\Omega - \Omega_0)}, \tag{3.27}$$

where

$$\mathbf{M}_{\mathscr{A}} = \begin{Vmatrix} 1 & a_1 & -\mathrm{e}^{2\mathrm{i}\Omega\beta' L_1} & 0 \\ 0 & a_2 & \mathrm{e}^{-2\mathrm{i}\Omega\beta' L_1} & -1 \\ 2\Omega h\beta & a_3 & 2\mathrm{i}\Omega h'\beta'\,\mathrm{e}^{2\mathrm{i}\Omega\beta' L_1} & 0 \\ 0 & a_4 & -2\mathrm{i}\Omega h'\beta'\,\mathrm{e}^{-2\mathrm{i}\Omega\beta' L_1} & 2\Omega h\beta \end{Vmatrix}. \tag{3.28}$$

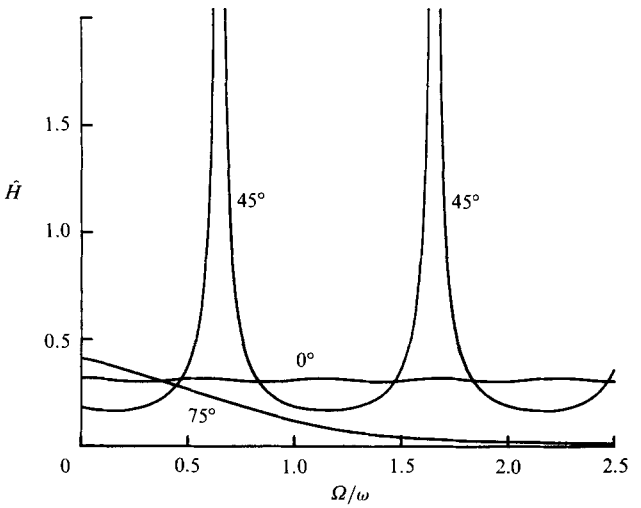

FIGURE 5. The frequency response, $\hat{\mathscr{H}}(2\Omega) = 2\Omega|\mathscr{H}|h/ga^2$, versus Ω/ω for collinear waves, $L/h = 10$, $\epsilon = 0.1$, $h'/h = 0.5$, $\sigma h = 1$ and three angles of incidence: (*a*) normal incidence ($\theta = 0°$); (*b*) $\theta = 45°$; and (*c*) $\theta = 75°$.

The special case of normal incidence ($\gamma = \nu = 0$), is qualitatively representative of all cases of small θ_e. Equation (3.8) is replaced by

$$\phi_{10}^{\mathrm{F}} = \phi_{10}^{F} = \mathrm{Re}\,\mathscr{G}\,\mathrm{e}^{-2\mathrm{i}\Omega[t_1+x_1/(gh)^{\frac{1}{2}}]} \qquad (x_1 < -L_1), \tag{3.29a}$$

$$\phi_{10}^{\mathrm{F}} = \phi_{10}^{G} + \phi_{10}^{K} \qquad (|x_1| < L_1), \tag{3.29b}$$

with

$$\phi_{10}^{H} = \mathrm{Re}\,\mathscr{H}\,\mathrm{e}^{-2\mathrm{i}\Omega[t_1-x_1/(gh')^{\frac{1}{2}}]}, \tag{3.29c}$$

$$\phi_{10}^{K} = \mathrm{Re}\,\mathscr{K}\,\mathrm{e}^{-2\mathrm{i}\Omega[t_1+x_1/(gh')^{\frac{1}{2}}]}, \tag{3.29d}$$

and

$$\phi_{10}^{\mathrm{F}} = \phi_{10}^{J} = \mathrm{Re}\,\mathscr{J}\,\mathrm{e}^{-2\mathrm{i}\Omega[t_1-x_1/(gh)^{\frac{1}{2}}]} \qquad (x_1 > -L_1). \tag{3.29e}$$

The free wave off the shelf is now propagating. Equations (3.20) and (3.21) are still valid if β is taken to be imaginary.

Figure 5 shows the dependence of $\hat{H} \equiv 2\Omega|H|h/ga^2$, which is the normalized amplitude of the trapped long wave, on Ω/ω, for collinear trains at various angles of incidence $\theta = \theta_e = \tan^{-1}\nu/\mu = \tan^{-1}\gamma/\alpha$. From (3.7) there are three regimes separated by the critical angles θ_1 and θ_2 corresponding respectively to $\beta^2 = 0$ and $\beta'^2 = 0$, i.e.

$$\sin\theta_1 = C_e/(gh)^{\frac{1}{2}}, \quad \sin\theta_2 = C_e/(gh')^{\frac{1}{2}}. \tag{3.30}$$

For $\theta_1 < \theta_e < \theta_2$, $-\beta^2$ is negative and β'^2 is positive; the free long waves are trapped on the shelf. Resonance occurs at frequencies given by (3.24); the spacing between them is simply $\pi/(4\beta' L_1)$. For $\theta_e < \theta_1$, both $-\beta^2$ and β'^2 are positive and the waves are propagating everywhere. No infinite resonance occurs, and the variation of the normalized $\hat{H}$ with respect to ΩL is uneventful. Finally, for $\theta_e > \theta_2$, both $-\beta^2$ and β'^2 are negative; the free long waves are evanescent on and off the shelf, as can be inferred from (3.23) and (3.28). $\hat{H}$ decays exponentially as ΩL increases.

In the case of non-collinear wavetrains the same three regimes exist and are determined by the signs of $-\beta^2$ and β'^2. These in turn are determined by the magnitude of $\nu^{-1} = C_e \sec\theta_e$ compared to $(gh)^{\frac{1}{2}}$ and $(gh')^{\frac{1}{2}}$. When θ_e is close to θ the resulting values are close to the results for collinear waves. When they differ, the qualitative behaviour is the same, and some quantitative variation occurs. Such

cases have been computed with results similar to those given in figure 4. We also note that the appearance of many zeros in figure 2 does not mean that the forcing of the free long waves vanishes. While they are oscillatory in kL, not all terms on the right of (3.1 *a*) vanish, nor are they in phase with respect to kL. The numerical values are, of course, functions of the short-wave scattering, which depend on the details of the topography, such as kL, the shape of the shelf edges, etc.

In the neighbourhood of the resonant peaks, the theory in this section breaks down. One way to achieve a uniformly valid theory is to examine the evolution over a much longer timescale $t_2 = \epsilon^2 t = O(1)$. Higher-order nonlinearity must then be invoked. In a related study of edge waves on a mild slope, Foda & Mei (1981) have derived a cubic Schrödinger equation for the resonated edge waves. Similar analysis would be dauntingly complex for the present problem. To avoid infinite resonance, one may alternatively examine incident wave packets of finite duration within the realm of $t_1 = O(1)$; the resonance peaks must then be finite.

4. Long waves due to an incident wave packet

4.1. *Normal incidence*

In the simplest case of normal incidence, trapping or resonance is not expected. Instead of the discrete-mode approach of §2, we view the short waves as sinusoidal waves modulated slowly in some general manner. Equations (2.6)–(2.8) hold near each edge with the coefficients A–E being functions of t_1, but the amplitudes D and E of waves propagating on the shelf must have different values at the two edges. In particular A, B, D and E in (2.6) must be evaluated at $x_1 = -L_1$, hence $A = A(-L_1, t_1)$ etc. On the other hand C, D and E in (2.7) must be evaluated at $x_1 = L_1$, hence $C = C(L_1, t_1)$ etc. Since $D = D(t_1 - x_1/C_g)$ and $E = E(t_1 + x_1/C_g)$ by the conservation of wave action, we have

$$D(L_1, t_1) = D(-L_1, t_1 - 2L_1/C_g), \quad E(-L_1, t_1) = E(L_1, t_1 + 2L_1/C_g). \tag{4.1}$$

With these relations and the prescribed $A(-L_1, t_1)$ we determine the short-wave amplitudes for each t_1: A, B, D and E at $x_1 = L_1$ and C, D and E at $x_1 = -L_1$. Subsequently, the locked long-waves are computed from these amplitudes through (3.1) and (3.3), and the Stokes' drift terms are found from (3.17). The results are lengthy and not presented here.

We now turn to the free long waves. In principle the values of ϕ_{10}^{F} at any point on the shelf can be calculated by the method of characteristics from the wave equations (3.5). However, much insight can be gained by a simpler calculation of the behaviour at the two edges only.

Instead of the sinusoidal dependence in (3.3) and (3.8), we now have

$$\left.\begin{aligned} &\phi_{10}^{Z} = \phi_{10}^{Z}(t_1 \mp x_1/C_g), && \text{for } Z = \begin{cases} A, C; \\ B, \end{cases} \\ \text{and} \quad &\phi_{10}^{Z} = \phi_{10}^{Z}(t_1 \mp x_1/C_g'), && \text{for } Z = \begin{cases} D, \\ E, \end{cases} \\ &\phi_{10}^{Z} = \phi_{10}^{Z}[t_1 \mp x_1/(gh)^{\frac{1}{2}}], && \text{for } Z = \begin{cases} J, \\ G, \end{cases} \\ \text{and} \quad &\phi_{10}^{Z} = \phi_{10}^{Z}[t_1 \mp x_1/(gh')^{\frac{1}{2}}], && \text{for } Z = \begin{cases} H, \\ K. \end{cases} \end{aligned}\right\} \tag{4.2}$$

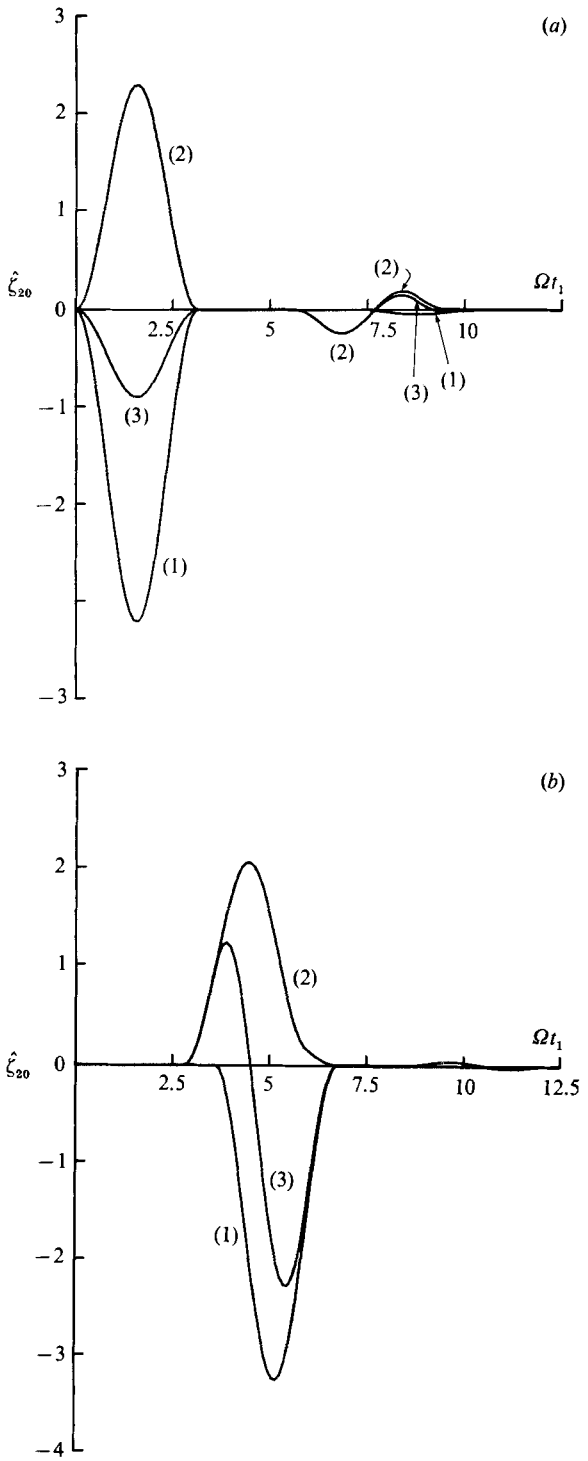

FIGURE 6. The normalized transient long-wave response $\zeta_{20} = h\zeta_{20}/a^2$, to normally incident waves, (*a*) at the left edge and (*b*) at the right edge of the shelf, for $h'/h = 0.5$, $L/h = 10$, $\sigma h = 1$, $\Omega/w = 1$. Curve (1) the locked waves, (2) the free waves, and (3) the total slow wave.

With this proviso (3.9), (3.18) and (3.19) are still formally valid. Using (4.2) we replace all the x_1 derivatives in (3.19*c*, *d*) by t_1 derivatives with appropriate constant multipliers. Equations (3.19*a–d*) then form a set of four first-order differential equations for ϕ_{10}^G, ϕ_{10}^H, ϕ_{10}^K and ϕ_{10}^J which can be integrated numerically with respect to time from $t_1 = 0$. The free long waves ϕ_{10}^Z at $-L_1$ and L_1 are thus determined.

In figure 6(*a*), we display the calculated long wave near the left edge. Note that the group-locked long wave which consists of both incident and reflected waves is a set-down while the radiated free long wave is a set-up. The net displacement of the two long waves is still a set-down. After $\Omega t_1 = 6$ reflection from the right edge returns to the left edge. The free long wave is now more dominant. The long wave at the right edge is shown in figure 6(*b*). The locked and free long waves are opposite in sign. Since the free long waves arrive earlier than the locked long waves, the total long wave is at first a set-up then a set-down.

4.2. *Oblique incidence and trapped waves*

For sufficiently oblique incidence, wave trapping occurs and ϕ_{10}^F becomes evanescent off the shelf. We shall use Fourier transformation of the incident-wave envelope in conjunction with the modulational frequency response to determine the transient envelope.

Because $\phi_{10_{t_1}}^F$ depends linearly on the incident-wave intensity $|A|^2$, we may construct the transient solution by the Fourier integral of the modulational frequency response. First, we define the Fourier integral representation of $|A|^2$ by

$$|A|^2 = \int_{-\infty}^{\infty} \mathrm{d}(2\Omega)\, \mathrm{e}^{-\mathrm{i}\tau(2\Omega)}\, \mathscr{S}_A(2\Omega), \tag{4.3}$$

where $\mathscr{S}_A$ is the Fourier spectrum of $|A|^2$. For illustration, let us consider a short-wave envelope which is itself a Gaussian wave packet with modulational frequency $\bar{\Omega}$:

$$A = A_0\, \mathrm{Re}\, \mathrm{e}^{-\mathrm{i}\bar{\Omega}\tau - \frac{1}{2}w^2\tau^2}, \tag{4.4}$$

where τ is the phase function

$$\tau = t_1 - \mu_1 x_1 - \nu y_1. \tag{4.5}$$

The Fourier spectrum is

$$\begin{aligned}\mathscr{S}_A &= \frac{1}{2\pi}\int_{-\infty}^{\infty} \mathrm{d}\tau\, \mathrm{e}^{2\mathrm{i}\Omega\tau}|A|^2 \\ &= \frac{1}{8w\pi^{\frac{1}{2}}}A_0^2[2\,\mathrm{e}^{-\Omega^2/w^2} + \mathrm{e}^{-(\Omega-\bar{\Omega})^2/w^2} + \mathrm{e}^{-(\Omega+\bar{\Omega})^2/w^2}].\end{aligned} \tag{4.6}$$

For an input of the form

$$\mathrm{Re}\,(\mathscr{A}\,\mathrm{e}^{-2\mathrm{i}\Omega\tau}) = \mathrm{Re}\,(\mathscr{A}^*\,\mathrm{e}^{2\mathrm{i}\Omega\tau}) \tag{4.7}$$

with $\Omega > 0$ we have already determined in §3.3 the free long waves $\mathscr{H}$ and $\mathscr{K}$ defined in (3.8*c*, *d*). We extend the definition of $\mathscr{H}(2\Omega)$ to $\Omega < 0$ using the fact that

$$\mathscr{H}(2\Omega) = \mathscr{H}^*(-2\Omega), \quad \mathscr{K}(2\Omega) = \mathscr{K}^*(-2\Omega), \tag{4.8}$$

which follows from (3.8*c*, *d*).

The transient response ζ_{20}^H, which represents the right-going free wave on the shelf is then constructed by Fourier superposition

$$\zeta_{20}^H(x_1, y_1, t_1) = \int_{-\infty}^{\infty} \mathrm{d}(2\Omega)\left(\frac{2\mathrm{i}\Omega}{g}\right)\mathscr{H}\, \mathrm{e}^{-2\mathrm{i}\Omega(t_1 - \beta' x_1 - \nu y_1)}, \tag{4.9}$$

where $\mathscr{H} = \mathscr{H}(2\Omega)$ is related to $\mathscr{A}(2\Omega)$ by (3.27) while $\mathscr{A}$ is given by (3.4) with A^+A^{-*} replaced by $\mathscr{S}_A$. Since $\mathscr{H}$ has poles at Ω_n the path of integration must be slightly above the real axis in the complex 2Ω-plane. The other free wave ζ_{20}^K can be represented similarly.

Sufficient insight can be gained by focusing attention on a point along the shelf axis. In the complex plane of 2Ω the function $\mathscr{H}(2\Omega)$ has real poles which correspond to the trapped modes. The transient response will be close to resonance if the forcing frequency Ω is close to one of the eigenfrequencies Ω_n. Let us assume that the forcing frequency $\overline{\Omega}$ coincides with the lowest eigenfrequency, corresponding to $n = 0$ in (3.4):

$$\overline{\Omega} = \Omega_0 = \frac{1}{2\beta' L_1} \tan^{-1}(\beta h/\beta' h'). \tag{4.10}$$

In the complex plane of 2Ω the integration path is slightly above the real axis in order that H tends to zero as t_1 goes to $-\infty$. Because of the Gaussian factors in (4.6) the integral in (4.9) derives most of its value when

$$\Omega \mp \overline{\Omega} = 0(w) \ll \Omega_0,$$

corresponding to the second and third terms in (4.6). Consider $x_1 = y_1 = 0$ only. Because of Hermitian symmetry of $\mathscr{S}_A$ and $\mathscr{H}$ in Ω we have

$$-g\zeta_{20}^H(0,0,t_1) \approx \frac{mA_0^2}{4w\pi^{\frac{1}{2}}} \operatorname{Re} \int_{-\infty}^{\infty} \mathrm{d}(2\Omega) \frac{\mathscr{H}_0}{2(\Omega - \Omega_0)} \mathrm{e}^{-2\mathrm{i}\Omega t_1 - (\Omega-\Omega_0)^2/w^2}, \tag{4.11}$$

where $\mathscr{H}_0\mathscr{A}$ is the residue of $\mathscr{H}$ at the pole at $\Omega = \Omega_0$ and is easily found from (3.27):

$$\mathscr{H}_0 = \mathbf{M}_{\Omega=\Omega_0}\{[(\beta h)^2 + (\beta' h')^2]\, 2\beta' L_1\, 4\Omega_0^2\}^{-1}. \tag{4.12}$$

Use has been made of the result

$$\mathscr{A}(2\Omega_0) = \frac{mA_0^2}{(-2\mathrm{i}\Omega)\, 8w\pi^{\frac{1}{2}}}. \tag{4.13}$$

The dependence of $\mathscr{H}_0$ on physical parameters will be discussed later.

The integral (4.11) can be analysed by the method of steepest descent (Carrier 1970). In the complex plane 2Ω, the phase function

$$\Gamma(2\Omega) = -2\mathrm{i}\Omega t_1 - \frac{(\Omega - \Omega_0)^2}{w^2} \tag{4.14}$$

has a saddle point at $\qquad 2\Omega = 2\Omega_0 - 2\mathrm{i}w^2 t_1$

which shifts downwards as t_1 increases. We transform the integration path to the path of steepest descent through the saddle point:

$$-g\zeta_{20}^H(0,0,t_1) \approx \frac{mA_0^2}{4w\pi^{\frac{1}{2}}} \operatorname{Re} \int_{-\infty-2\mathrm{i}w^2 t_1}^{\infty-2\mathrm{i}w^2 t_1} \mathrm{d}(2\Omega) \frac{\mathscr{H}_0}{2(\Omega-\Omega_0)} \mathrm{e}^{-2\mathrm{i}\Omega t_1 - (\Omega-\Omega_0)^2/w^2}$$

$$+ \mathbb{H}(t_1) \operatorname{Re}\left[-2\pi\mathrm{i} \frac{\mathscr{H}_0}{4w\pi^{\frac{1}{2}}} \mathrm{e}^{-2\mathrm{i}\Omega_0 t_1} \right]. \tag{4.15}$$

The last term, which includes the Heaviside step function $\mathbb{H}$, arises from the pole at Ω_0. By the following change of variable:

$$\sigma = 2\Omega - 2\Omega_0 + 2\mathrm{i}w^2 t_1$$

the integral in (4.15) becomes

$$\mathscr{H}_0 \, \mathrm{e}^{-w^2 t_1^2 - 2\mathrm{i}\Omega_0 t_1} \int_{-\infty}^{\infty} \mathrm{d}\sigma \frac{\mathrm{e}^{-\sigma^2/4w^2}}{\sigma - 2\mathrm{i}w^2 t_1}, \tag{4.16}$$

which has been evaluated by Carrier (1970) as

$$\mathscr{H}_0 \operatorname{sgn}(t_1) \mathrm{i}\pi \, \mathrm{e}^{-w^2 t_1^2} [1 - \operatorname{erf} w|t_1|]. \tag{4.17}$$

Equations (4.15) and (4.17) can now be combined to give finally

$$-g\zeta_{20}^H(0,0,t_1) \approx \operatorname{Re} \frac{\mathrm{i}\pi^{\frac{1}{2}} m A_0^2}{4w} \mathscr{H}_0 \{\operatorname{sgn}(t_1)[1 - \operatorname{erf} w|t_1|] - 2\mathbb{H}(t_1)\} \, \mathrm{e}^{-2\mathrm{i}\Omega_0 t_1}. \tag{4.18}$$

In view of (3.25) the left-going component $-g\zeta_{20}^K(0,0,t_1)$ on the shelf is given simply by (4.18) with $\mathscr{H}_0$ replaced by $-\mathscr{H}_0^*$.

The strength of the transient response (4.18) depends on the energy in the input packet via the packet length $1/w$, and on the residue $\mathscr{H}_0$. The normalized forcing

$$\hat{\mathscr{H}}_0 = 2\Omega_0 |\mathscr{H}_0 \mathscr{A}| (h/g)^{\frac{3}{2}}/a^2 \tag{4.19}$$

and the normalized resonance frequency

$$\hat{\Omega}_0 = \Omega_0 (h/g)^{\frac{1}{2}} \tag{4.20}$$

are plotted as functions of the envelope incidence angle θ_e in figure 7 (*a*) for collinear waves and in figure 7 (*b*) for non-collinear waves with $\theta_e - \theta = 60°$. The angular spread corresponding to the latter case can be inferred from (2.13), where Ω is now equal to the resonance frequency Ω_0 which also depends on θ, θ_e and h'/h. As noted before, Ω_0 (hence trapping and resonance) exists only in the range $\theta_1 < \theta_e < \theta_2$, where θ_1 and θ_2 are defined in (3.30). As can be seen in these figures the collinear and non-collinear cases are qualitatively similar. The range of trapping $\theta_2 - \theta_1$ is smaller for larger h'/h and also for larger $\theta_e - \theta$. From (4.10) we can verify that as $\theta_e \downarrow \theta_1, \beta \downarrow 0$ so that $\Omega_0 \downarrow 0$, and as $\theta_e \uparrow \theta_2, \beta' \downarrow 0$ so that $\Omega_0 \uparrow \infty$. From (4.12) we can also see that as $\theta_e \uparrow \theta_2, \mathscr{H}_0 \uparrow \infty$ since $\beta' \downarrow 0$. As $\theta \downarrow \theta_1$ we see by substituting $\Omega = 0$ in (3.22) that

$$a_3 \to h'\mathscr{U}^{(2)} - h\mathscr{U}^{(1)}; \quad a_4 \to h\mathscr{U}^{(4)} - h'\mathscr{U}^{(3)}. \tag{4.21}$$

Letting β and Ω_0 be small in (3.28) we find by using (4.21) that to the leading order in β' and Ω_0

$$\begin{aligned} M &\to 2\mathrm{i}\Omega_0 h' b' (a_4 - a_3) \\ &\to 2\mathrm{i}\Omega_0 h'\beta' [h(\mathscr{U}^{(1)} + \mathscr{U}^{(4)} - h'(\mathscr{U}^{(2)} + \mathscr{U}^{(3)})]. \end{aligned} \tag{4.22}$$

It follows from (4.12) and (4.19) that

$$\hat{H}_0 \to [h(\mathscr{U}^{(1)} + \mathscr{U}^{(4)}) - h'(\mathscr{U}^{(2)} + \mathscr{U}^{(3)})] \left(\frac{h}{g}\right)^{\frac{3}{2}} \Big/ (2a^2 h'\beta'^2 L_1). \tag{4.23}$$

Because the Stokes' drift terms do not depend on Ω and remain finite as $\Omega \downarrow 0$, this forcing for the resonated shelf wave is finite at $\theta_e = \theta_1$, as shown in figure 7 (*a*, *b*). The singular limit at $\theta_e = \theta_2$ corresponds to an envelope caustic; further refinement of the present theory is required but is not pursued here.

Figure 8 (*a*, *b*) shows an example of $\zeta_{20}^H(0,0,t_1)$ due to the transient input of (4.4), for two different values of w. As can be seen there is a transition through which the

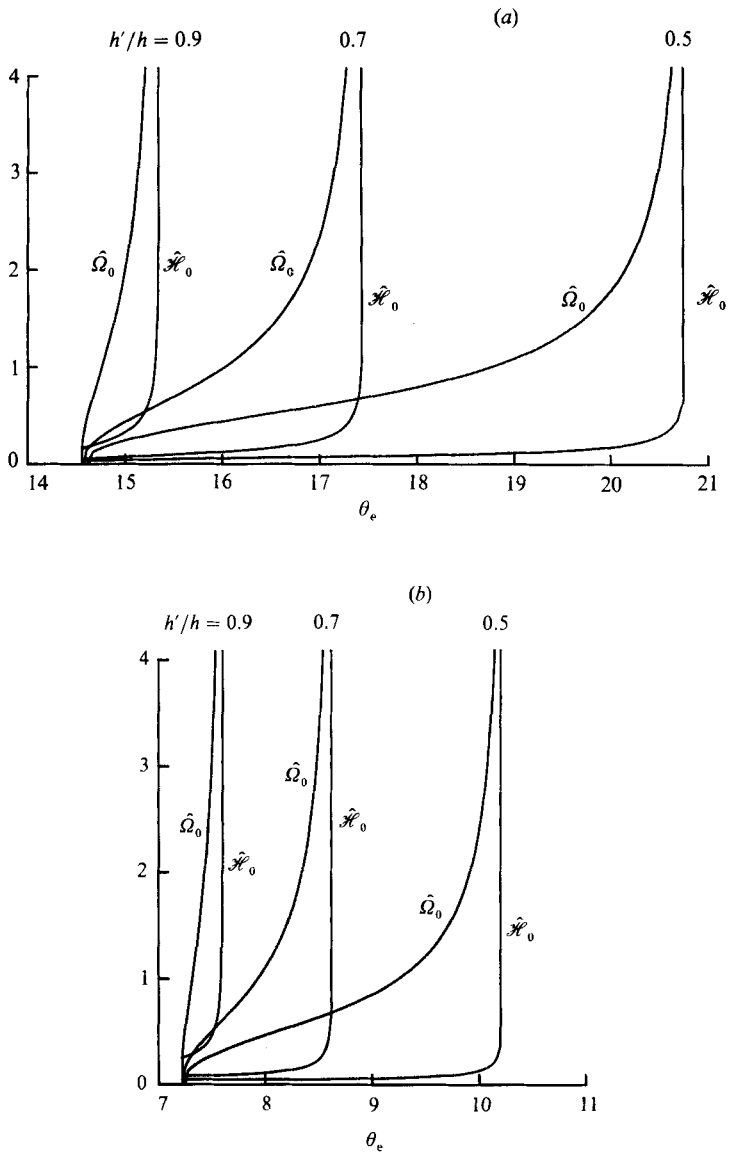

FIGURE 7. The resonance frequency $\hat{\Omega}_0 = \Omega_0(h/g)^{\frac{1}{2}}$ at which the first pole occurs and the normalized residue of $\hat{\mathscr{H}}_0 = 2\Omega_0|\mathscr{H}_0\mathscr{A}|(h/g)^{\frac{3}{2}}/a^2$, the residue at Ω_0 *vs.* θ_e for $L/h = 10$, $\sigma h = 4$, and three depth ratios: $h'/h = 0.5$, 0.7, 0.9; (*a*) collinear incidence: $\theta_e = \theta$; (*b*) non-collinear incidence: $\theta = \theta_e - 60°$.

free long wave builds up before the arrival of the peak of the envelope. Afterwards the incident wave packet moves away along the positive y_1 axis and leaves a steady 'wake' of reverberation which is an oscillation at the resonance frequency. The parameter $1/w$ is proportional to the total duration of the incident wave packet. The amplitude of reverberation decreases for increasing w. If w is very small the realm of validity of the present theory will be exceeded. Higher-order effects must then be accounted for.

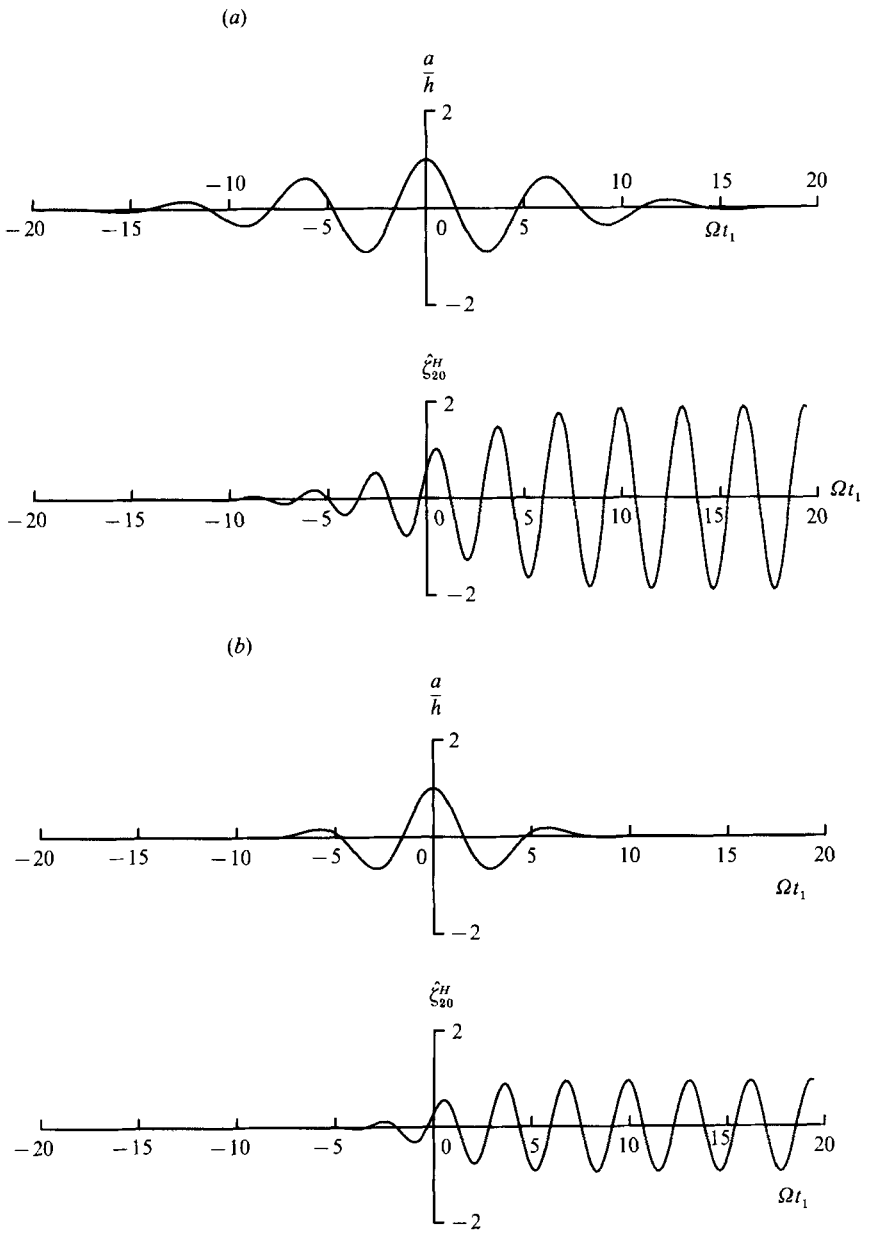

FIGURE 8. Transient response to an obliquely incident wave packet. The normalized incident short-wave amplitude a/h (where ϵa is the physical amplitude) and the value of $\hat{\zeta}^H_{20} = \zeta^H_{20}(0, 0, t_1)$ $2\Omega h/ga^2$ are plotted versus Ωt_1. Collinear incidence with $\theta_e = \theta = 45°$, $h'/h = 0.5$, $L/h = 10$, $\sigma h = 1$. The computed $\Omega_0 = 0.65$ and $\mathscr{H}_0 h/a^2 = 0.17 - 0.12\mathrm{i}$. (*a*) $w = 0.1$; (*b*) $w = 0.2$.

5. Concluding remarks

In this paper a problem of nonlinear diffraction of slowly modulated short waves by a wide ridge has been studied by combining the tools of matched asymptotics and multiple scales. Everywhere in the fluid there are two timescales: the short wave period and the long group period. In the near field of each edge there is only one

spatial scale, i.e. the short wavelength, and both propagating and evanescent modes are important. In the far field away from the edges, there are two spatial scales, but only the propagating part of the short waves matters. Two kinds of long waves must be present: one is locked to the short-wave groups and one is propagating at the local speed of the shallow-water wave. When the angle of incidence is sufficiently oblique, the second long wave can be trapped on the ridge which then becomes a wave guide. If the incident wave is a packet with a finite length in the direction of propagation, a persistent wake of reverberation can be resonated along the ridge.

There are other situations where long-wave excitation can be of great practical interest. In many small harbours the lowest natural modes have periods of 5–20 minutes. In view of the analysis of this paper, these long-period harbour modes can be resonated by short wind waves nonlinearly, in addition to the linear resonance by tsunamis. This has indeed been reported in some harbours, but effective calculations still await further studies.

We thank the financial support of the US Office of Naval Research (Contract N00014-80-C-531-NR (433 2-228) and US National Science Foundation (Grant MEA 8400649). Y. Agnon also acknowledges the support from Gershon Meirbaum Foundation, WHOI and Fulbright foundation during his graduate study in the WHOI/MIT Joint Program.

REFERENCES

AGNON, Y. & MEI, C. C. 1985 Slow drift motion of a two-dimensional block in beam seas. *J. Fluid Mech.* **151**, 279–294.

CARRIER, G. F. 1970 The dynamics of tsunamis. *Mathematical Problems in Geophysical Fluid Dynamics*, pp. 157–181. American Mathematical Society, Providence, RI.

FODA, M. A. & MEI, C. C. 1981 Nonlinear excitation of long trapped waves by a group of short swells. *J. Fluid Mech.* **111**, 319–345.

GARRETT, C. J. R. 1971 Wave forces on a circular dock. *J. Fluid Mech.* **46**, 129–139.

LONGUET-HIGGINS, M. S. 1967 On the trapping of wave energy round islands. *J. Fluid Mech.* **29**, 781–821.

MEI, C. C. 1983 *Applied Dynamics of Ocean Surface Waves.* Wiley Interscience.

MEI, C. C. & BENMOUSSA, C. 1984 Long waves induces by short-wave groups over an uneven bottom. *J. Fluid Mech.* **139**, 219–235.

MEI, C. C. & BLACK, J. L. 1969 Scattering of surface waves by rectangular obstacles in waters of finite depth. *J. Fluid Mech.* **38**, 499–511.

MILES, J. W. 1967 Surface wave scattering matrix for a shelf. *J. Fluid Mech.* **28**, 755–767.

NEWMAN, J. N. 1965 Propagation of water waves past long two dimensional obstacles. *J. Fluid Mech.* **23**, 23–29.